Systematic study of α decay half-lives for even-even nuclei within a two-potential approach

Xiao-Dong Sun,[1] Ping Guo,[1] and Xiao-Hua Li[2,3,*]

[1]*School of Math and Physics, University of South China, 421001 Hengyang, People's Republic of China*

[2]*School of Nuclear Science and Technology, University of South China, 421001 Hengyang, People's Republic of China*

[3]*Cooperative Innovation Center for Nuclear Fuel Cycle Technology & Equipment, University of South China, 421001 Hengyang, People's Republic of China*

(Received 17 November 2015; revised manuscript received 30 January 2016; published 15 March 2016)

α decay is a common and important process of natural radioactivity of heavy and superheavy nuclei. The α decay half-lives for even-even nuclei from $Z = 62$ to $Z = 118$ are systematically studied based on the two-potential approach with a quasistationary state approximation. As for the nuclear potential, the isospin effect is considered, which slightly improves the results by 6.8%. To reduce the deviations between experimental half-lives and calculated results due to the nuclear shell structure, the analytic expression of hindrance factors is employed. Our results can reproduce the experimental half-lives as good as using the density-dependent cluster model and the generalized liquid drop model.

DOI: 10.1103/PhysRevC.93.034316

I. INTRODUCTION

Transuranic elements follow the trend that their half-lives decrease as the atomic numbers increase until the next nuclear shell appears. Synthesized atoms of the most recently discovered 117 element have lasted some tens of microseconds [1,2], gradually approaching the island of the stable superheavy element [3]. One of useful ways to confirm the superheavy elements is to discriminate specific α particles emanated from itself as well as its α decay chain nuclei. Landing the island of stability and other interesting discoveries, such as the triplet shape coexistence [4] and extremely long α decay half-life nuclide ^{209}Bi [5] and so on, has made experimental and theoretical research on α decay one of the hottest topics again.

In 1928, Gurney and Condon [6] and Gamow [7] independently put forward the quantum tunnel theory, which successfully estimated the probability of an α particle tunneling through the Coulomb barrier. The process of barrier tunneling (penetration) is one important assumption for α decay. The other is that α particle clusters are prone to forming on the surface of the parent nucleus. The underlying problem is that before the α particle in the bound state collides with the barrier, we know little of how the α particle forms and little about the motion inside the parent nucleus. The difficulties come from the complicated structure of the quantum many-body systems, e.g., the collective deformation, the nuclear shell closure, and the uncertainty of nuclear potential between the α particle and the remaining nucleus.

Recently, many kinds of models were proposed to deal with the process of α decay, such as the cluster model [8–10], the liquid drop model [11–15], the unified model for α decay and α capture [16,17], the empirical formulas [18–22], and others [23–29]. The nuclear potential plays a key role in both the assault frequency and the penetration probability. The double-folding model adopting the density-dependent M3Y force has been used in the density-dependent cluster model [9,10]. At the same time, the proximity potential related to surface nucleons has been employed by the generalized liquid drop model (GLDM) [13–15] and by the Coulomb and proximity models [24]. The coupled-channels method has also been used to interpret the fine structure of α decay [27]. Usually, the α particle preformation probabilities were taken as constant [8,10,13], but they would abruptly decrease near the nuclear shell closures, in fact, due to the deficiency of the valence nucleons or holes [30–32]. Fortunately on the one hand the effective preformation probabilities can be extracted from the ratios of the calculated α decay half-lives to the experimental data [15,31–35]. On the other hand the microscopic shell model plus cluster component can provide the preformation probability successfully [36–40].

In this work we focus on predicting the α decay half-life more accurately and studying the isospin effect of the nuclear potential. We adopt the two-potential approach with a quasistationary state approximation [23] and draw on the analytic expression for the α particle preformation probability in Ref. [15] to estimate variation of the hindrance factors with the number of valence nucleon. The model parameters are obtained by fitting 164 α decay half-lives of even-even nuclei taken from the newest nuclear property table NUBASE2012 [41].

This article is organized as follows. In Sec. II the theoretical framework of α decay half-lives and the analytic expression for α particle preformation hindrance factors are briefly described. In Sec. III we present the numerical results and discussion of the hindrance factor and the isospin effect of the nuclear potential. A brief summary is given in Sec. IV.

II. THEORETICAL FRAMEWORK

The half-life $T_{1/2}$ for α decay could be determined by the α decay width Γ or the decay constant λ. It can be written as

$$T_{1/2} = \frac{\hbar ln2}{\Gamma} = \frac{ln2}{\lambda}. \quad (1)$$

*Corresponding author: lixiaohuaphysics@126.com

The decay constant λ depending on the α particle preformation probability P_α, the penetration probability P, and the normalized factor F, which represents the collision probability or assault frequency, can be expressed as

$$\lambda = \frac{P_\alpha F P}{h}, \tag{2}$$

where $h = \frac{T^{\rm exp}_{1/2}}{T^{\rm cal}_{1/2}}$ is defined as the hindrance factor. The superscripts "exp" and "cal" represent experimental data and calculated values, respectively. The normalized factor F, which is given by the integration over the internal region [23], can be written as

$$F \int_{r_1}^{r_2} \frac{dr}{2k(r)} = 1, \tag{3}$$

where r is the mass center distance between the preformed α particle and the daughter nucleus, and r_1 and r_2 and following r_3 are the classical turning points. $k(r) = \sqrt{\frac{2\mu}{\hbar^2}|Q_\alpha - V(r)|}$ is the wave number. μ is the reduced mass of the α particle and the daughter nucleus in the center-of-mass coordinate. $V(r)$ and Q are the height of the α core potential and the α decay energy, respectively. The penetration probability P, which is calculated by the WKB approximation, can be expressed as

$$P = \exp\left[-2\int_{r_2}^{r_3} k(r)dr\right]. \tag{4}$$

The classical turning points satisfy the condition $V(r_1) = V(r_2) = V(r_3) = Q$. In the inner region $(r_1 < r < r_2)$ the strong interaction commands the state of the preformed α particle, while in the outer region $(r_2 < r < r_3)$ the electromagnetic interaction plays a major role.

The potential between the preformed α particle and the daughter nucleus, including nuclear, Coulomb, and centrifugal potential barriers, can be written as

$$V(r) = V_N(r) + V_C(r) + V_l(r), \tag{5}$$

where $V_N(r)$ represents the nuclear potential. In this work, we choose a type of cosh parametrized form for the nuclear potential [42]. It can be expressed as

$$V_N(r) = -V_0 \frac{1 + \cosh(R/a)}{\cosh(r/a) + \cosh(R/a)}, \tag{6}$$

where V_0 and a are parameters of the depth and diffuseness for the nuclear potential, respectively. $V_C(r)$ is the Coulomb potential and is taken as the potential of a uniformly charged sphere with the sharp radius R, which can be expressed as

$$V_C(r) = \begin{cases} \frac{Z_d Z_\alpha e^2}{2R}\left[3 - \left(\frac{r}{R}\right)^2\right], & r < R, \\ \frac{Z_d Z_\alpha e^2}{r}, & r > R, \end{cases} \tag{7}$$

where Z_d and Z_α are proton number of the daughter nucleus and the α particle, respectively. The sharp radius R is given by

$$R = 1.28A^{1/3} - 0.76 + 0.8A^{-1/3}. \tag{8}$$

This empirical formula is commonly used to calculate α decay half-lives [13], which derive from the nuclear droplet model and the proximity energy. $V_l(r) = \frac{l(l+1)\hbar^2}{2\mu r^2}$ is the centrifugal potential, where l is the orbital angular momentum taken away by the α particle. In general, only the favored transitions ($l = 0$) take place for α decay of even-even nuclei [15], and then $V_l(r) = 0$.

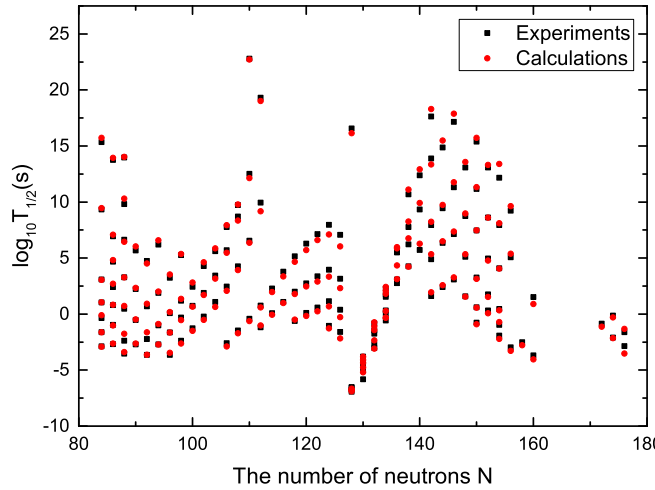

FIG. 1. Logarithmic of half-lives as a function of neutron numbers of parent nuclei. The black squares and red circles represent the experimental data and the calculated results, respectively.

The hindrance factor h reflects the deviations between the half-lives $T^{\rm cal}_{1/2}$ calculated with the constant preformation probability P_α and the experimental data $T^{\rm exp}_{1/2}$. It systematically varies due to the nuclear shell effect. The trend of the hindrance factor h can be estimated by the simple formula with five parameters proposed by Zhang *et al.* to research how the preformation probability of α particle varies in the different nuclear shells [15,33]. The hindrance factor can be given by

$$\log_{10} h = a + b(Z - Z_1)(Z_2 - Z) + c(N - N_1)(N_2 - N) + dA + e(Z - Z_1)(N - N_1), \tag{9}$$

where Z, N, and A are the proton, neutron, and mass numbers of the parent nucleus. Z_1 and Z_2 (N_1 and N_2) are the proton (neutron) magic numbers around Z (N). a, b, c, d, and

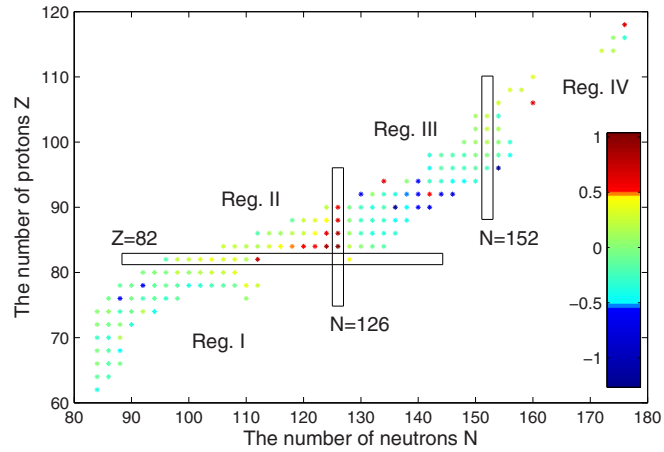

FIG. 2. Logarithmic of deviation on a color map as a function of neutron numbers N and proton numbers Z of the parent nuclei.

e are the adjustable parameters. In Eq. (9), the first and fourth terms describe the magnitude and the trend of the preformation probability with the increasing mass number, the second and third terms show a parabolic dependence of $\log_{10} h$ as a function of the valence proton (neutron) number, and the last term relates to the integrated valence neutron-proton interaction strength [15,34].

III. RESULTS AND DISCUSSIONS

The experimental data includes 164 even-even nuclei from $Z = 62$ to $Z = 118$, whose α decay energy Q_α and half-lives $T_{1/2}^{\exp}$ are taken from AME2012 [43,44] and NUBASE2012 [41], respectively. In the present work, the preformation factor P_0 is taken as 0.43 for even-even nuclei in accordance with the density-dependent cluster model (DDCM) [10]. The nuclear potential is given as in Eq. (6) with adjustable parameters, the depth V_0 and the diffuseness a. The parameters can be obtained by fitting the experimental half-lives to minimize the total square deviation Δ, which is defined as

$$\Delta = \sum_{i=1}^{N} \left(\log_{10} T_{1/2}^{\text{cal}} - \log_{10} T_{1/2}^{\exp} \right)^2. \tag{10}$$

Then we discuss the influence of the isospin effect on the nuclear potential and study the hindrance factors due to the nuclear shell.

A. Isospin effect of the nuclear potential

From the term of the symmetry energy in the Bethe-Weizsäcker mass formula [45] and the asymmetry-dependent components in the nucleon-nucleon optical model [46], we can see that they both show that the isospin effect plays a role in nuclear physics. The excited analog state in the nuclei and the exotic phenomenon of neutron-proton pairing could also be isospin related [47]. Neutrons and protons have been treated as being different charge states of the same particles, but the fact that the strong interaction is independent of charge leads to confusion regarding the origin and to uncertainty of the isospin effect [48,49].

The α particle tends to preform on the surface of the decaying nucleus. If protons and neutrons distribute in different nucleonic density the asymmetry of the isospin may affect the motion of α particles, and the collective nuclear potential between the α particle and the core may be isospin dependent. Without considering the isospin effect, a set of appropriate parameters can be obtained by fitting the α decay half-lives of 164 even-even nuclei, i.e., $a = 0.5966$ fm and $V_0 = 194.37$ MeV. And the root-mean-square (rms) deviation is $\sqrt{\frac{\Delta}{164}} = 0.369$. Using the set of parameters we systematically calculate the α decay half-lives, which are listed in the third column in Table III. All the half-lives are in the unit of seconds. While considering the isospin effect of the nuclear potential, we add a parameter related to the isospin in the depth of the nuclear potential in the form of the Lane potential [50]. By fitting the same database of 164 nuclei, the isospin-dependent nuclear potential could be given as

$$V_0 = 192.42 + 31.059 \frac{N - Z}{A} \text{ MeV},$$
$$a = 0.5958 \text{ fm}. \tag{11}$$

The rms deviation drops to $\sqrt{\frac{\Delta}{164}} = 0.344$. From the rms deviations, we can find that the calculated results considering the isospin effect of the nuclear potential slightly improve by $\frac{0.369-0.344}{0.369} = 6.8\%$, which is consistent with Ref. [51]. The calculated α decay half-lives are shown in the fourth column

TABLE I. Comparison of the fit error of magic numbers for superheavy nuclei to the α particle preformation probabilities.

Region	Number	Z_1	Z_2	N_1	N_2	$\overline{\sigma^2}$
I	61	50	82	82	126	0.0358
II	26	82	126	82	126	0.0159
II	26	82	120	82	126	0.0159
II	26	82	114	82	126	0.0160
III	59	82	126	126	152	0.0495
III	59	82	120	126	152	0.0496
III	59	82	114	126	152	0.0498
IV	13	82	126	152	184	0.0131
IV	13	82	120	152	172	0.0129
IV	13	82	114	152	184	0.0129

TABLE II. The parameters of hindrance factors for even-even nuclei from four different regions. Region I is $50 < Z \leqslant 82$ and $82 < N \leqslant 126$, Region II is $82 < Z \leqslant 126$ and $82 < N \leqslant 126$, Region III is $82 \leqslant Z \leqslant 126$ and $126 < N \leqslant 152$, and Region IV is $82 < Z \leqslant 126$ and $152 < N \leqslant 184$.

Region	a	b	c	d	e
I	−0.265	−0.0009	−0.0016	0.0035	0.0008
II	2.8205	−0.0028	−0.0022	−0.0078	0.0005
III	15.2472	0.0011	−0.0004	−0.0717	0.0052
IV	−20.731	0.0026	−0.0007	0.0766	−0.0027

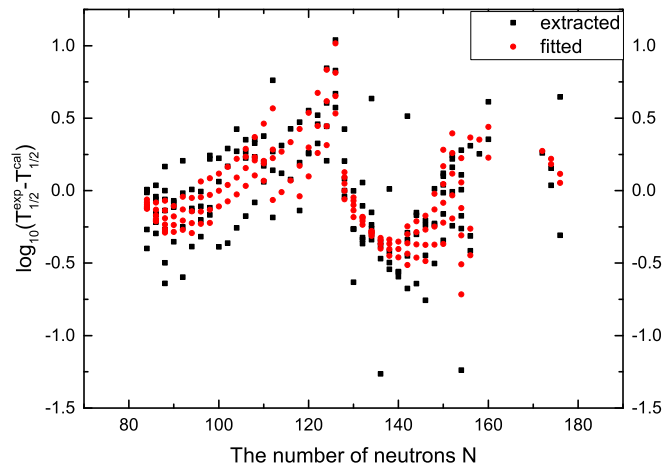

FIG. 3. Logarithmic of hindrance factors as a function of neutron numbers of the parent nuclei. The black squares and red circles represent the extracted data and the fitted results, respectively.

TABLE III. Comparisons among experimental α decay half-lives $T_{1/2}^{\rm exp}$ and calculated results within this work, using the generalized liquid drop model $T_{1/2}^{\rm GLDM}$ [55], the density-dependent cluster model $T_{1/2}^{\rm DDCM}$ [10,56] of even-even nuclei with proton numbers $Z = 62$–118. $T_{1/2}^{\rm cal2}$ and $T_{1/2}^{\rm cal3}$ represent the calculated half-lives using the two-potential approach without and with the isospin-dependent nuclear potential, respectively. The star in $T_{1/2}^{\rm cal3*}$ denotes taking into account the variations of hindrance factors. All the half-lives are in the unit of seconds.

Nuclei	$T_{1/2}^{\rm exp}$ (s)	$T_{1/2}^{\rm cal2}$ (s)	$T_{1/2}^{\rm cal3}$ (s)	$T_{1/2}^{\rm cal3*}$ (s)	$T_{1/2}^{\rm GLDM}$ (s)	$T_{1/2}^{\rm DDCM}$ (s)
^{146}Sm	2.20×10^{15}	5.51×10^{15}	5.50×10^{15}	3.89×10^{15}	13×10^{15}	2.3×10^{15}
^{148}Gd	2.20×10^{9}	2.87×10^{9}	3.12×10^{9}	2.38×10^{9}	6.4×10^{9}	1.7×10^{9}
^{150}Gd	5.60×10^{13}	9.23×10^{13}	9.88×10^{13}	5.77×10^{13}	22×10^{13}	6.0×10^{13}
^{150}Dy	1.20×10^{3}	1.18×10^{3}	1.20×10^{3}	9.98×10^{2}	2.4×10^{3}	0.83×10^{3}
^{152}Dy	8.60×10^{6}	1.26×10^{7}	1.59×10^{7}	1.26×10^{7}	25×10^{6}	8.5×10^{6}
^{154}Dy	9.50×10^{13}	1.09×10^{14}	1.23×10^{14}	5.17×10^{13}	20×10^{13}	5.1×10^{13}
^{152}Er	1.10×10^{1}	1.13×10^{1}	1.17×10^{1}	9.50×10^{0}	2.1×10^{1}	0.86×10^{1}
^{154}Er	4.80×10^{4}	6.93×10^{4}	4.45×10^{4}	4.09×10^{4}	7.4×10^{4}	3.1×10^{4}
^{156}Er	6.70×10^{9}	2.10×10^{10}	2.22×10^{10}	1.52×10^{10}	39×10^{9}	–
^{154}Yb	4.40×10^{-1}	8.14×10^{-1}	4.31×10^{-1}	3.85×10^{-1}	6.9×10^{-1}	3.4×10^{-1}
^{156}Yb	2.60×10^{2}	5.13×10^{2}	5.61×10^{2}	3.70×10^{2}	8.7×10^{2}	4.0×10^{2}
^{158}Yb	4.30×10^{6}	2.93×10^{6}	3.27×10^{6}	1.71×10^{6}	4.5×10^{6}	2.0×10^{6}
^{156}Hf	2.40×10^{-2}	2.42×10^{-2}	2.43×10^{-2}	1.75×10^{-2}	3.5×10^{-2}	1.5×10^{-2}
^{158}Hf	6.40×10^{0}	7.03×10^{0}	7.49×10^{0}	6.05×10^{0}	11×10^{0}	5.6×10^{0}
^{160}Hf	1.90×10^{3}	1.90×10^{3}	2.20×10^{3}	1.29×10^{3}	2.7×10^{3}	1.6×10^{3}
^{162}Hf	4.90×10^{5}	1.10×10^{6}	1.09×10^{6}	6.21×10^{5}	15×10^{5}	8.2×10^{5}
^{158}W	1.30×10^{-3}	1.28×10^{-3}	1.38×10^{-3}	1.31×10^{-3}	2×10^{-3}	0.9×10^{-3}
^{160}W	1.10×10^{-1}	1.01×10^{-1}	1.19×10^{-1}	8.84×10^{-2}	1.6×10^{-1}	0.82×10^{-1}
^{162}W	3.00×10^{0}	5.56×10^{0}	3.75×10^{0}	2.77×10^{0}	5.9×10^{0}	3.3×10^{0}
^{164}W	1.70×10^{2}	2.20×10^{2}	2.61×10^{2}	1.46×10^{2}	3.1×10^{2}	2.0×10^{2}
^{166}W	5.50×10^{4}	3.42×10^{4}	5.02×10^{4}	1.93×10^{4}	4.1×10^{4}	2.8×10^{4}
^{168}W	1.60×10^{6}	3.89×10^{6}	3.96×10^{6}	2.18×10^{6}	4.6×10^{6}	–
^{162}Os	2.10×10^{-3}	2.40×10^{-3}	2.30×10^{-3}	1.95×10^{-3}	3.6×10^{-3}	1.8×10^{-3}
^{164}Os	4.10×10^{-3}	1.79×10^{-2}	2.44×10^{-2}	1.70×10^{-2}	31×10^{-3}	1.8×10^{-3}
^{166}Os	3.00×10^{-1}	3.53×10^{-1}	5.30×10^{-1}	3.19×10^{-1}	4.9×10^{-1}	3.7×10^{-1}
^{168}Os	4.90×10^{0}	8.71×10^{0}	8.30×10^{0}	5.24×10^{0}	9.1×10^{0}	6.5×10^{0}
^{170}Os	7.80×10^{1}	1.07×10^{2}	1.41×10^{2}	6.92×10^{1}	14×10^{1}	10×10^{1}
^{172}Os	1.70×10^{3}	3.53×10^{3}	3.43×10^{3}	2.15×10^{3}	3.9×10^{3}	3.3×10^{3}
^{174}Os	1.80×10^{5}	2.36×10^{5}	2.58×10^{5}	1.47×10^{5}	2.8×10^{5}	2.4×10^{5}
^{186}Os	6.30×10^{22}	5.48×10^{22}	7.81×10^{22}	5.66×10^{22}	10×10^{22}	4.2×10^{22}
^{166}Pt	3.00×10^{-4}	4.12×10^{-4}	3.28×10^{-4}	2.85×10^{-4}	4.5×10^{-4}	2.3×10^{-4}
^{168}Pt	2.00×10^{-3}	2.40×10^{-3}	2.34×10^{-3}	1.86×10^{-3}	3.3×10^{-3}	1.8×10^{-3}
^{170}Pt	6.00×10^{-3}	2.37×10^{-2}	2.32×10^{-2}	1.54×10^{-2}	26×10^{-3}	18×10^{-3}
^{172}Pt	1.00×10^{-1}	1.33×10^{-1}	1.38×10^{-1}	9.32×10^{-2}	1.6×10^{-1}	1.2×10^{-1}
^{174}Pt	1.20×10^{0}	1.54×10^{0}	1.59×10^{0}	1.21×10^{0}	1.7×10^{0}	1.5×10^{0}
^{176}Pt	1.60×10^{1}	2.36×10^{1}	2.45×10^{1}	1.85×10^{1}	2.6×10^{1}	2.5×10^{1}
^{178}Pt	2.70×10^{2}	6.60×10^{2}	6.03×10^{2}	6.76×10^{2}	5.8×10^{2}	2.5×10^{2}
^{180}Pt	1.90×10^{4}	4.38×10^{4}	2.81×10^{4}	1.97×10^{4}	2.3×10^{4}	2.7×10^{4}
^{182}Pt	4.20×10^{5}	7.58×10^{5}	9.66×10^{5}	6.93×10^{5}	7.9×10^{5}	9.4×10^{5}
^{184}Pt	5.89×10^{7}	8.83×10^{7}	1.05×10^{8}	9.29×10^{7}	10×10^{7}	12×10^{7}
^{186}Pt	5.30×10^{9}	6.39×10^{9}	7.00×10^{9}	7.28×10^{9}	7.1×10^{9}	8.6×10^{9}
^{188}Pt	3.30×10^{12}	1.39×10^{12}	1.38×10^{12}	1.98×10^{12}	1.6×10^{12}	1.7×10^{12}
^{190}Pt	2.00×10^{19}	1.07×10^{19}	1.09×10^{19}	1.97×10^{19}	1.8×10^{19}	1.7×10^{19}
^{172}Hg	2.30×10^{-4}	2.40×10^{-4}	2.73×10^{-4}	3.01×10^{-4}	3.9×10^{-4}	2.4×10^{-4}
^{174}Hg	2.00×10^{-3}	1.96×10^{-3}	1.87×10^{-3}	2.02×10^{-3}	2.6×10^{-3}	1.9×10^{-3}
^{176}Hg	2.30×10^{-2}	2.33×10^{-2}	2.34×10^{-2}	3.01×10^{-2}	2.9×10^{-2}	2.4×10^{-2}
^{178}Hg	5.00×10^{-1}	3.02×10^{-1}	4.24×10^{-1}	2.93×10^{-1}	3.5×10^{-1}	3.2×10^{-1}
^{180}Hg	5.40×10^{0}	4.67×10^{0}	6.15×10^{0}	4.49×10^{0}	5.2×10^{0}	5.5×10^{0}
^{182}Hg	7.80×10^{1}	5.30×10^{1}	2.76×10^{2}	5.34×10^{1}	5.6×10^{1}	6.5×10^{1}
^{184}Hg	2.80×10^{3}	1.50×10^{3}	2.07×10^{3}	2.04×10^{3}	1.6×10^{3}	2.1×10^{3}
^{186}Hg	5.00×10^{5}	2.98×10^{5}	3.22×10^{5}	4.56×10^{5}	3.0×10^{5}	4.2×10^{5}
^{188}Hg	5.20×10^{8}	2.30×10^{8}	2.63×10^{8}	3.71×10^{8}	2.4×10^{8}	3.4×10^{8}
^{178}Pb	2.30×10^{-4}	3.66×10^{-4}	2.05×10^{-4}	2.31×10^{-4}	3.0×10^{-4}	–

TABLE III. (*Continued.*)

Nuclei	$T_{1/2}^{\mathrm{exp}}$ (s)	$T_{1/2}^{\mathrm{cal2}}$ (s)	$T_{1/2}^{\mathrm{cal3}}$ (s)	$T_{1/2}^{\mathrm{cal3*}}$ (s)	$T_{1/2}^{\mathrm{GLDM}}$ (s)	$T_{1/2}^{\mathrm{DDCM}}$ (s)
^{180}Pb	4.20×10^{-3}	2.40×10^{-3}	2.74×10^{-3}	2.98×10^{-3}	3.2×10^{-3}	–
^{182}Pb	5.50×10^{-2}	3.29×10^{-2}	6.56×10^{-2}	3.97×10^{-2}	3.9×10^{-2}	5.7×10^{-2}
^{184}Pb	6.10×10^{-1}	3.12×10^{-1}	3.58×10^{-1}	4.89×10^{-1}	3.6×10^{-1}	4.0×10^{-1}
^{186}Pb	1.20×10^{1}	4.52×10^{0}	5.07×10^{0}	5.97×10^{0}	4.4×10^{1}	0.52×10^{1}
^{188}Pb	2.80×10^{2}	1.25×10^{2}	1.42×10^{2}	2.19×10^{2}	1.1×10^{2}	1.5×10^{2}
^{190}Pb	1.80×10^{4}	8.48×10^{3}	9.08×10^{3}	1.72×10^{4}	0.76×10^{4}	1.0×10^{4}
^{192}Pb	3.50×10^{6}	2.36×10^{6}	4.39×10^{6}	1.68×10^{7}	2.0×10^{6}	2.8×10^{6}
^{194}Pb	8.80×10^{9}	1.52×10^{9}	2.29×10^{9}	4.62×10^{9}	1.4×10^{9}	1.9×10^{9}
^{210}Pb	3.70×10^{16}	1.39×10^{16}	1.35×10^{16}	2.38×10^{16}	2.0×10^{16}	1.1×10^{16}
^{190}Po	2.50×10^{-3}	1.35×10^{-3}	1.50×10^{-3}	3.61×10^{-3}	1.7×10^{-3}	1.9×10^{-3}
^{192}Po	3.40×10^{-2}	1.99×10^{-2}	2.89×10^{-2}	2.26×10^{-2}	2.2×10^{-2}	2.8×10^{-2}
^{194}Po	3.90×10^{-1}	2.47×10^{-1}	3.33×10^{-1}	3.46×10^{-1}	2.5×10^{-1}	3.9×10^{-1}
^{196}Po	5.70×10^{0}	4.13×10^{0}	4.34×10^{0}	6.05×10^{0}	3.6×10^{0}	6.3×10^{0}
^{198}Po	1.90×10^{2}	9.28×10^{1}	1.51×10^{2}	1.68×10^{2}	0.81×10^{2}	1.6×10^{2}
^{200}Po	6.20×10^{3}	2.32×10^{3}	2.92×10^{3}	4.60×10^{3}	2.0×10^{3}	4.2×10^{3}
^{202}Po	1.40×10^{5}	4.71×10^{4}	6.58×10^{4}	1.16×10^{5}	0.38×10^{5}	0.87×10^{5}
^{204}Po	1.90×10^{6}	5.32×10^{5}	5.97×10^{5}	3.04×10^{6}	0.45×10^{6}	1.1×10^{6}
^{206}Po	1.40×10^{7}	4.22×10^{6}	3.91×10^{6}	1.86×10^{7}	0.30×10^{7}	0.70×10^{7}
^{208}Po	9.10×10^{7}	1.30×10^{7}	1.55×10^{7}	8.18×10^{7}	0.12×10^{7}	2.8×10^{7}
^{210}Po	1.20×10^{7}	1.10×10^{6}	1.19×10^{6}	1.08×10^{7}	0.092×10^{7}	0.23×10^{7}
^{212}Po	3.00×10^{-7}	1.87×10^{-7}	1.85×10^{-7}	2.14×10^{-7}	2.5×10^{-7}	2.3×10^{-7}
^{214}Po	1.60×10^{-4}	1.60×10^{-4}	2.16×10^{-4}	1.51×10^{-4}	1.6×10^{-4}	2.3×10^{-4}
^{216}Po	1.50×10^{-1}	1.91×10^{-1}	2.00×10^{-1}	1.16×10^{-1}	1.5×10^{-1}	2.4×10^{-1}
^{218}Po	1.90×10^{2}	2.68×10^{2}	2.93×10^{2}	1.28×10^{2}	2.1×10^{2}	3.5×10^{2}
^{198}Rn	6.60×10^{-2}	1.01×10^{-1}	9.40×10^{-2}	7.48×10^{-2}	8.1×10^{-2}	–
^{200}Rn	1.20×10^{0}	9.09×10^{-1}	1.02×10^{0}	9.26×10^{-1}	0.83×10^{0}	1.7×10^{0}
^{202}Rn	1.20×10^{1}	1.00×10^{1}	9.56×10^{0}	1.16×10^{1}	0.71×10^{1}	1.8×10^{1}
^{204}Rn	1.00×10^{2}	6.41×10^{1}	7.23×10^{1}	1.04×10^{2}	0.49×10^{2}	1.3×10^{2}
^{206}Rn	5.50×10^{2}	3.05×10^{2}	3.05×10^{2}	6.12×10^{2}	2.1×10^{2}	6.0×10^{2}
^{208}Rn	2.40×10^{3}	8.35×10^{2}	1.14×10^{3}	2.76×10^{3}	0.65×10^{3}	1.9×10^{3}
^{210}Rn	8.91×10^{3}	2.22×10^{3}	2.49×10^{3}	9.27×10^{3}	1.6×10^{3}	5.0×10^{3}
^{212}Rn	1.40×10^{3}	2.08×10^{2}	2.39×10^{2}	1.25×10^{3}	0.15×10^{3}	0.50×10^{3}
^{214}Rn	2.70×10^{-7}	2.24×10^{-7}	2.27×10^{-7}	2.31×10^{-7}	2.9×10^{-7}	2.8×10^{-7}
^{216}Rn	4.50×10^{-5}	8.25×10^{-5}	8.76×10^{-5}	1.06×10^{-4}	8.2×10^{-5}	11×10^{-5}
^{218}Rn	3.50×10^{-2}	8.12×10^{-2}	7.63×10^{-2}	4.33×10^{-2}	5.3×10^{-2}	9.2×10^{-2}
^{220}Rn	5.60×10^{1}	1.22×10^{2}	1.46×10^{2}	7.16×10^{1}	8.8×10^{1}	17×10^{1}
^{222}Rn	3.30×10^{5}	7.43×10^{5}	8.31×10^{5}	3.01×10^{5}	6.3×10^{5}	10×10^{5}
^{206}Ra	2.40×10^{-1}	3.29×10^{-1}	2.81×10^{-1}	2.74×10^{-1}	2.1×10^{-1}	4.6×10^{-1}
^{208}Ra	1.30×10^{0}	7.12×10^{-1}	8.27×10^{-1}	1.06×10^{0}	0.57×10^{0}	1.4×10^{0}
^{210}Ra	3.80×10^{0}	1.79×10^{0}	2.14×10^{0}	3.42×10^{0}	1.3×10^{0}	3.3×10^{0}
^{212}Ra	1.40×10^{1}	5.05×10^{0}	5.28×10^{0}	1.32×10^{1}	0.33×10^{1}	9.2×10^{1}
^{214}Ra	2.50×10^{0}	5.36×10^{-1}	5.97×10^{-1}	2.20×10^{0}	0.41×10^{0}	1.3×10^{0}
^{216}Ra	1.80×10^{-7}	1.80×10^{-7}	1.84×10^{-7}	1.76×10^{-7}	2.5×10^{-7}	2.5×10^{-7}
^{218}Ra	2.50×10^{-5}	4.60×10^{-5}	5.15×10^{-5}	4.00×10^{-5}	4.7×10^{-5}	6.7×10^{-5}
^{220}Ra	1.80×10^{-2}	3.79×10^{-2}	3.54×10^{-2}	2.33×10^{-2}	2.5×10^{-2}	4.8×10^{-2}
^{222}Ra	3.40×10^{1}	6.81×10^{1}	8.23×10^{1}	4.41×10^{1}	4.5×10^{1}	10×10^{1}
^{224}Ra	3.20×10^{5}	9.42×10^{5}	9.69×10^{5}	3.69×10^{5}	5.1×10^{5}	7.7×10^{5}
^{226}Ra	5.00×10^{10}	1.32×10^{11}	1.98×10^{11}	5.37×10^{10}	15×10^{10}	12.4×10^{10}
^{214}Th	8.70×10^{-2}	5.42×10^{-2}	5.96×10^{-2}	1.05×10^{-1}	0.04×10^{-2}	10×10^{-2}
^{216}Th	2.60×10^{-2}	6.94×10^{-3}	8.44×10^{-3}	2.63×10^{-2}	0.62×10^{-2}	–
^{218}Th	1.20×10^{-7}	1.32×10^{-7}	1.81×10^{-7}	1.26×10^{-7}	2.2×10^{-7}	1.3×10^{-7}
^{220}Th	9.70×10^{-6}	1.79×10^{-5}	2.13×10^{-5}	1.62×10^{-5}	20×10^{-6}	18×10^{-6}
^{222}Th	2.10×10^{-3}	4.56×10^{-3}	6.13×10^{-3}	2.42×10^{-3}	3.0×10^{-3}	3.5×10^{-3}
^{224}Th	1.10×10^{0}	1.89×10^{0}	2.23×10^{0}	1.28×10^{0}	1.3×10^{0}	1.4×10^{0}
^{226}Th	1.20×10^{3}	2.20×10^{4}	5.16×10^{3}	2.19×10^{3}	2.8×10^{3}	2.1×10^{3}
^{228}Th	6.00×10^{7}	1.88×10^{8}	2.15×10^{8}	1.15×10^{8}	13×10^{7}	7.6×10^{7}

TABLE III. (*Continued.*)

Nuclei	$T_{1/2}^{\mathrm{exp}}$ (s)	$T_{1/2}^{\mathrm{cal2}}$ (s)	$T_{1/2}^{\mathrm{cal3}}$ (s)	$T_{1/2}^{\mathrm{cal3*}}$ (s)	$T_{1/2}^{\mathrm{GLDM}}$ (s)	$T_{1/2}^{\mathrm{DDCM}}$ (s)
^{230}Th	2.40×10^{12}	8.69×10^{12}	9.12×10^{12}	3.30×10^{12}	8.7×10^{12}	3.0×10^{12}
^{232}Th	4.40×10^{17}	2.08×10^{18}	2.53×10^{18}	6.35×10^{17}	33×10^{17}	6.5×10^{17}
^{222}U	1.51×10^{-6}	6.48×10^{-6}	7.51×10^{-6}	4.01×10^{-6}	6.3×10^{-6}	3.7×10^{-6}
^{224}U	9.40×10^{-4}	8.26×10^{-4}	9.89×10^{-4}	4.47×10^{-4}	6.2×10^{-4}	8.0×10^{-4}
^{226}U	2.70×10^{-1}	4.94×10^{-1}	7.18×10^{-1}	2.77×10^{-1}	3.2×10^{-1}	3.6×10^{-1}
^{228}U	5.70×10^{2}	1.36×10^{3}	1.22×10^{3}	6.76×10^{2}	6.1×10^{2}	5.2×10^{2}
^{230}U	1.70×10^{6}	5.93×10^{6}	5.78×10^{6}	2.40×10^{6}	3.1×10^{6}	4.3×10^{6}
^{232}U	2.20×10^{9}	8.64×10^{9}	8.13×10^{9}	3.38×10^{9}	5.1×10^{9}	5.1×10^{9}
^{234}U	7.70×10^{13}	2.36×10^{13}	2.85×10^{13}	1.00×10^{13}	2.4×10^{12}	14×10^{12}
^{236}U	7.40×10^{14}	3.24×10^{15}	8.06×10^{15}	8.90×10^{14}	32×10^{14}	14×10^{14}
^{238}U	1.40×10^{17}	7.98×10^{17}	1.17×10^{18}	2.16×10^{17}	11×10^{17}	3.3×10^{17}
^{228}Pu	2.10×10^{0}	4.86×10^{-1}	6.03×10^{-1}	2.73×10^{-1}	0.29×10^{0}	–
^{232}Pu	1.80×10^{4}	1.75×10^{4}	2.01×10^{4}	1.11×10^{4}	0.91×10^{4}	1.2×10^{4}
^{234}Pu	5.30×10^{5}	1.93×10^{6}	1.39×10^{6}	5.31×10^{5}	6.1×10^{5}	6.2×10^{5}
^{236}Pu	9.00×10^{7}	1.75×10^{8}	2.11×10^{8}	9.82×10^{7}	11×10^{7}	12×10^{7}
^{238}Pu	2.80×10^{9}	5.61×10^{9}	7.40×10^{9}	3.03×10^{9}	3.7×10^{9}	3.4×10^{9}
^{240}Pu	2.10×10^{11}	5.88×10^{11}	6.88×10^{11}	3.30×10^{11}	4.7×10^{11}	3.2×10^{11}
^{242}Pu	1.20×10^{13}	3.82×10^{13}	5.26×10^{13}	1.43×10^{13}	3.2×10^{13}	1.8×10^{13}
^{244}Pu	2.50×10^{15}	5.50×10^{15}	6.57×10^{15}	2.46×10^{15}	7.5×10^{15}	2.9×10^{15}
^{238}Cm	7.90×10^{4}	2.23×10^{5}	2.13×10^{5}	1.61×10^{5}	8.5×10^{4}	–
^{240}Cm	2.30×10^{6}	3.26×10^{6}	3.69×10^{6}	1.93×10^{6}	1.5×10^{6}	2.1×10^{6}
^{242}Cm	1.40×10^{7}	2.42×10^{7}	2.56×10^{7}	1.23×10^{7}	1.1×10^{7}	1.5×10^{7}
^{244}Cm	5.70×10^{8}	9.60×10^{8}	1.25×10^{9}	5.63×10^{8}	5.2×10^{8}	5.4×10^{8}
^{246}Cm	1.50×10^{11}	2.17×10^{11}	3.09×10^{11}	1.52×10^{11}	1.8×10^{11}	1.3×10^{11}
^{248}Cm	1.20×10^{13}	2.10×10^{13}	2.60×10^{13}	1.35×10^{13}	2×10^{13}	1.1×10^{13}
^{250}Cm	1.50×10^{12}	2.60×10^{13}	2.70×10^{13}	3.60×10^{12}	18×10^{12}	8.6×10^{12}
^{240}Cf	4.10×10^{1}	8.92×10^{1}	1.04×10^{2}	5.33×10^{1}	3.5×10^{1}	–
^{242}Cf	2.60×10^{2}	3.84×10^{2}	5.09×10^{2}	2.53×10^{2}	1.7×10^{2}	3.0×10^{2}
^{244}Cf	1.20×10^{3}	1.93×10^{3}	2.45×10^{3}	1.35×10^{3}	0.82×10^{3}	1.4×10^{3}
^{246}Cf	1.30×10^{5}	2.24×10^{5}	1.89×10^{5}	1.17×10^{5}	0.64×10^{5}	1.1×10^{5}
^{248}Cf	2.90×10^{7}	3.00×10^{7}	3.56×10^{7}	2.35×10^{7}	1.4×10^{7}	1.9×10^{7}
^{250}Cf	4.10×10^{8}	4.17×10^{8}	5.12×10^{8}	3.71×10^{8}	2.3×10^{8}	2.5×10^{8}
^{252}Cf	8.60×10^{7}	1.28×10^{8}	1.58×10^{8}	4.99×10^{7}	7.3×10^{7}	8.3×10^{7}
^{254}Cf	1.70×10^{9}	4.42×10^{9}	5.32×10^{9}	1.84×10^{9}	2.9×10^{9}	2.8×10^{9}
^{248}Fm	3.80×10^{1}	3.69×10^{1}	5.13×10^{1}	3.60×10^{1}	1.5×10^{1}	2.5×10^{1}
^{250}Fm	1.80×10^{3}	1.43×10^{3}	1.65×10^{3}	1.55×10^{3}	0.54×10^{3}	1.0×10^{3}
^{252}Fm	9.10×10^{4}	6.27×10^{4}	7.77×10^{4}	7.34×10^{4}	2.1×10^{4}	3.7×10^{4}
^{254}Fm	1.20×10^{4}	1.18×10^{4}	1.69×10^{4}	7.36×10^{3}	0.42×10^{4}	0.74×10^{4}
^{256}Fm	1.20×10^{5}	2.46×10^{5}	2.01×10^{5}	1.04×10^{5}	0.6×10^{5}	1.1×10^{5}
^{252}No	4.10×10^{0}	3.74×10^{0}	3.27×10^{0}	3.84×10^{0}	1.1×10^{0}	2.1×10^{0}
^{254}No	5.70×10^{1}	3.44×10^{1}	4.69×10^{1}	5.42×10^{1}	1.1×10^{1}	2.3×10^{1}
^{256}No	2.90×10^{0}	2.26×10^{0}	2.04×10^{0}	1.70×10^{0}	0.7×10^{0}	1.3×10^{0}
^{254}Rf	1.70×10^{-1}	1.29×10^{-1}	1.91×10^{-1}	2.56×10^{-1}	0.6×10^{-1}	0.35×10^{-1}
^{256}Rf	2.10×10^{0}	1.20×10^{0}	1.06×10^{0}	3.03×10^{0}	0.34×10^{0}	0.68×10^{0}
^{258}Rf	1.10×10^{-1}	2.01×10^{-1}	1.63×10^{-1}	1.59×10^{-1}	0.55×10^{-1}	0.65×10^{-1}
^{260}Sg	1.20×10^{-2}	6.30×10^{-3}	7.54×10^{-3}	1.45×10^{-2}	0.29×10^{-2}	0.45×10^{-2}
^{266}Sg	3.30×10^{1}	8.04×10^{0}	9.57×10^{0}	1.29×10^{1}	0.15×10^{1}	0.82×10^{1}
^{264}Hs	1.10×10^{-3}	5.39×10^{-4}	5.91×10^{-4}	1.13×10^{-3}	0.25×10^{-3}	0.54×10^{-3}
^{266}Hs	3.10×10^{-3}	1.73×10^{-3}	2.40×10^{-3}	3.64×10^{-3}	0.86×10^{-3}	1.8×10^{-3}
^{270}Ds	2.10×10^{-4}	9.28×10^{-5}	1.07×10^{-4}	2.15×10^{-4}	0.57×10^{-4}	0.64×10^{-4}
^{286}Fl	1.40×10^{-1}	7.67×10^{-2}	9.16×10^{-2}	1.50×10^{-1}	0.24×10^{-1}	3.3×10^{-1}
^{288}Fl	7.50×10^{-1}	5.24×10^{-1}	7.01×10^{-1}	9.86×10^{-1}	1.2×10^{-1}	16×10^{-1}
^{290}Lv	8.00×10^{-3}	7.34×10^{-3}	1.14×10^{-2}	1.29×10^{-2}	2.7×10^{-3}	26×10^{-3}
^{292}Lv	2.40×10^{-2}	4.87×10^{-2}	2.89×10^{-2}	3.42×10^{-2}	0.79×10^{-2}	7.6×10^{-2}
^{294}118	1.40×10^{-3}	3.15×10^{-4}	3.61×10^{-4}	3.66×10^{-4}	0.14×10^{-3}	1.2×10^{-3}

of Table III. This set of isospin-dependent parameters is used to calculate the hindrance factors in the following.

B. Hindrance factors and systematic calculation of half-lives

Based on the set of isospin-dependent nuclear potential parameters, we calculate the α decay half-lives. Systematic variations of the half-lives as a function of the neutron numbers N of the parent nuclei are shown in Fig. 1. The black squares and red circles represent experimental half-lives and calculated ones, respectively. As we can see the theoretical results can well reproduce the experimental data of the α decay half-lives, although the magnitude of half-lives varies in a very wide range from 10^{-7} to 10^{22} s. It is noticed that the α decay half-life $T_{1/2}$ is extremely sensitive to the decay energy Q_α; for example, the decay energy, increasing 2.6 times results in 18 orders of magnitude shorter half-life for $N = 84$ isotones. A decrease in the symmetry energy may be responsible for the weakened stability [52].

Furthermore, it is obvious that the size of the deviation between experimental half-lives and calculated results roughly increases with the increasing valence nucleons especially for nuclides with $N = 82$–126. To more clearly show the results, the deviations for 164 nuclei are plotted as a color map in Fig. 2. The complete area is divided into four regions by the spherical magic numbers $Z = 82$ and $N = 126$ and the deformed magic number $N = 152$ [33]. The logarithmic of deviations in the area close to the magic number are greater than the mean value, indicating the calculated half-lives are small and suggesting the preformation factor P_0 is too large for the closed shell nuclei. This rule is significant in particular for spherical magic numbers $Z = 82$ and $N = 126$, where clustering induced by the pairing mode is inhibited [31]. In general, the calculated half-lives are relatively large for nuclei in Regions I and III. In other words, the preformation probabilities in Regions I and III are greater than those in Regions II and IV. The reason why the preformation probabilities in Region II are small may be that the nuclei are close to the magic numbers $Z = 82$ and $N = 126$. The reason for small preformation probabilities in Region IV may be that the nuclei are approaching the next proton and neutron shell closures, such as the doubly magic spherical nuclei at ($Z = 114$, $N = 184$), ($Z = 120$, $N = 172$), or at ($Z = 126$, $N = 184$) [53], and then the shell effect appears again.

The α particle preformation probabilities could be hindered by the nuclear shell closures. To predict the trends of the α particle preformation probabilities, the extracted hindrance factors are characterized using the analytic expression of Eq. (9), which has taken into account the nuclear shell effect and the proton-neutron interaction. $Z = 50$ and 82, and $N = 82$, 126, and 184 are well-known magic numbers for neutrons and protons. However, we do not know exactly the magic number for superheavy nuclei, and the predicted proton and neutron magic numbers for superheavy nuclei depend on the models and force parameters. According to the investigation within various parametrizations of relativistic and nonrelativistic nuclear mean-field models and the predictions in Ref. [53], we fit the extracted preformation probabilities with different proton magic numbers, and the results are listed in Table I. The fit is defined as $\overline{\sigma^2} = \frac{1}{n}\sum_{i=1}^{n}(y_{\rm fit} - y_{\rm data})^2$. The fit of ($Z = 114$, $N = 184$) is the worst in Regions II and III, indicating that $Z = 114$ is unlikely to be the next proton magic number in this region, which is consistent with the result in Ref. [54]. The next proton magic number after $Z = 82$ may be $Z = 126$.

The obtained parameters of Eq. (9) are listed in Table II. The extracted hindrance factors and the fitted ones as a function of neutron numbers N are shown in Fig. 3. As we can see the trend for fitted hindrance factors is similar to the extracted ones. Based on the improvement of hindrance factors, our results can reproduce the experimental half-lives within a factor of 2 for most nuclei, and the rms deviation drops to $\sqrt{\frac{\Delta}{164}} = 0.199$. The calculated half-lives can be found in the fifth column in Table III.

As can be seen from Table II, the absolute values of parameters b and c in Region II are both maximum, showing the preformation probabilities in Region II are strongly parabolic due to these nuclei sandwiched between magic numbers $Z = 82$ and $N = 126$. And it is interesting that parameter d is negatively correlated with parameters a and e. When the term of nuclei mass A makes greater contributions to the hindrance factors in different regions, the contributions from the constant term and the valence neutron-proton term are smaller, which shows that these three terms are related. A physical explanation of this relationship closely associated with the nucleons clustering in heavy nuclei is worth exploring in the future.

In Table III, we show the experimental α decay half-lives and calculated results of even-even nuclei with proton numbers $Z = 62$–118. The first column denotes the parent nucleus. The second column expresses the experimental half-lives of α decay. The next two columns indicate calculated results using the two-potential approach, and the superscript 2 or 3 marks the number of parameters of the nuclear potential without or with the isospin effect. The star means taking into account the correction of hindrance factors. For comparison, the calculated half-lives using the GLDM and the DDCM are also listed in the last two columns, respectively. In general, our results are as good as the others, especially for the nuclei around the shell closures, considering the correction of hindrance factors. The rms deviations between the calculated half-lives and the experimental data using different models are listed in Table IV for comparison.

To appraise the role of correction of hindrance factors, we plot the deviations between the calculated and experimental half-lives again in Fig. 4. Compared with Fig. 2, the abrupt increasing of the deviations close to the magic number has been resolved.

TABLE IV. The rms deviations between the experimental data and the calculated half-lives using the GLDM, the DDCM, and the two-potential approach.

	GLDM	DDCM	This work
rms	0.492	0.275	0.199

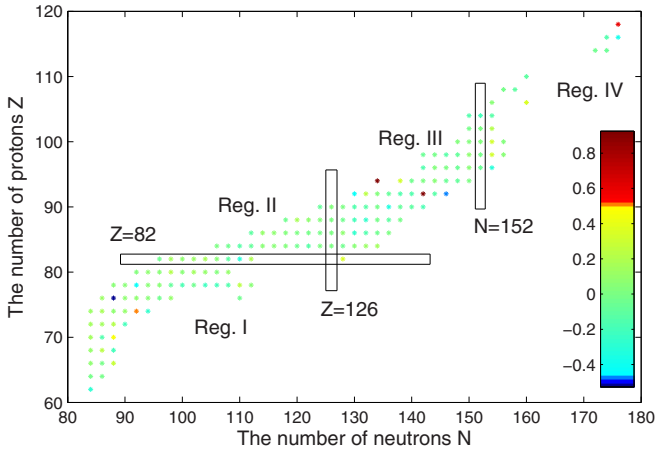

FIG. 4. Logarithmic of deviation on a color-map as a function of neutron numbers N and proton numbers Z of the parent nuclei considering the hindrance factors.

IV. SUMMARY

In summary, we systematically calculate the α decay half-lives for even-even nuclei with proton numbers from $Z = 62$ to $Z = 118$ using the two-potential approach based on the isospin-dependent nuclear potential taking into account the hindrance factors. A set of new parameters of isospin-dependent nuclear potentials and analytic expression of hindrance factors is obtained by fitting to the experimental half-lives. Numerical results can well reproduce the experimental half-lives compared with the DDCM and the GLDM, eliminating the shortcoming that the calculated results deteriorated in the vicinity of the magic number. The isospin effect on the α core nuclear potential can slightly improve the calculated results.

ACKNOWLEDGMENTS

We thank Professor H. F. Zhang for kindly discussion and comments. This work is supported in part by the National Natural Science Foundation of China (Grant No.11205083), the construct program of the key discipline in hunan province, the Research Foundation of Education Bureau of Hunan Province,China (Grant No.15A159), the Natural Science Foundation of Hunan Province, China (Grant No.2015JJ3103),the Innovation Group of Nuclear and Particle Physics in USC, Hunan Provincial Innovation Foundation For Postgraduate (Grant No.CX2015B398).

[1] Y. T. Oganessian, F. S. Abdullin, C. Alexander, J. Binder, R. A. Boll, S. Dmitriev, J. Ezold, K. Felker, J. Gostic, R. Grzywacz *et al.*, Phys. Rev. Lett. **109**, 162501 (2012).
[2] J. Khuyagbaatar, A. Yakushev, C. E. Düllmann, D. Ackermann, L.-L. Andersson, M. Asai, M. Block, R. Boll, H. Brand, D. Cox *et al.*, Phys. Rev. Lett. **112**, 172501 (2014).
[3] S. Hofmann and G. Münzenberg, Rev. Mod. Phys. **72**, 733 (2000).
[4] A. Andreyev, M. Huyse, P. Van Duppen, L. Weissman, D. Ackermann, J. Gerl, F. Hessberger, S. Hofmann, A. Kleinböhl, G. Münzenberg *et al.*, Nature (London) **405**, 430 (2000).
[5] P. De Marcillac, N. Coron, G. Dambier, J. Leblanc, and J.-P. Moalic, Nature (London) **422**, 876 (2003).
[6] R. W. Gurney and E. U. Condon, Nature (London) **122**, 439 (1928).
[7] G. Gamow, Z. Phys. **51**, 204 (1928).
[8] B. Buck, A. C. Merchant, and S. M. Perez, Phys. Rev. Lett. **65**, 2975 (1990).
[9] C. Xu and Z. Ren, Phys. Rev. C **74**, 014304 (2006).
[10] C. Xu and Z. Ren, Nucl. Phys. A **760**, 303 (2005).
[11] D. Poenaru, M. Ivascu, and A. Sandulescu, J. Phys. G **5**, L169 (1979).
[12] M. Goncalves and S. B. Duarte, Phys. Rev. C **48**, 2409 (1993).
[13] G. Royer, J. Phys. G **26**, 1149 (2000).
[14] H. Zhang, W. Zuo, J. Li, and G. Royer, Phys. Rev. C **74**, 017304 (2006).
[15] S. Guo, X. Bao, Y. Gao, J. Li, and H. Zhang, Nucl. Phys. A **934**, 110 (2015).
[16] P. Mohr, Phys. Rev. C **73**, 031301 (2006).
[17] V. Y. Denisov, O. I. Davidovskaya, and I. Y. Sedykh, Phys. Rev. C **92**, 014602 (2015).
[18] H. Geiger and J. Nuttall, Philos. Mag. Ser. 6 **22**, 613 (1911).
[19] Y. Ren and Z. Ren, Phys. Rev. C **85**, 044608 (2012).
[20] D. Poenaru, R. Gherghescu, and W. Greiner, J. Phys. G **39**, 015105 (2012).
[21] D. S. Delion, Phys. Rev. C **80**, 024310 (2009).
[22] Z. Wang, Z. Niu, Q. Liu, and J. Guo, J. Phys. G **42**, 055112 (2015).
[23] S. A. Gurvitz and G. Kalbermann, Phys. Rev. Lett. **59**, 262 (1987).
[24] K. Santhosh, I. Sukumaran, and B. Priyanka, Nucl. Phys. A **935**, 28 (2015).
[25] A. Zdeb, M. Warda, and K. Pomorski, Phys. Rev. C **87**, 024308 (2013).
[26] O. Tavares, E. Medeiros, and M. L. Terranova, J. Phys. G **31**, 129 (2005).
[27] D. Ni and Z. Ren, Phys. Rev. C **81**, 064318 (2010).
[28] C. Qi, A. Andreyev, M. Huyse, R. J. Liotta, P. Van Duppen, and R. Wyss, Phys. Lett. B **734**, 203 (2014).
[29] D. S. Delion, in *Theory of Particle and Cluster Emission* (Springer, Berlin, 2010), pp. 93–105.
[30] P. E. Hodgson and E. Běták, Phys. Rep. **374**, 1 (2003).
[31] C. Qi, F. R. Xu, R. J. Liotta, and R. Wyss, Phys. Rev. Lett. **103**, 072501 (2009).
[32] Y. Qian and Z. Ren, Sci. China: Phys., Mech. Astron. **56**, 1520 (2013).
[33] H. F. Zhang, G. Royer, Y. J. Wang, J. M. Dong, W. Zuo, and J. Q. Li, Phys. Rev. C **80**, 057301 (2009).
[34] G. Gangopadhyay, J. Phys. G **36**, 095105 (2009).
[35] W. Seif, Phys. Rev. C **91**, 014322 (2015).
[36] K. Varga, R. G. Lovas, and R. J. Liotta, Phys. Rev. Lett. **69**, 37 (1992).
[37] R. G. Lovas, R. Liotta, A. Insolia, K. Varga, and D. Delion, Phys. Rep. **294**, 265 (1998).
[38] D. S. Delion and R. J. Liotta, Phys. Rev. C **87**, 041302 (2013).
[39] R. I. Betan and W. Nazarewicz, Phys. Rev. C **86**, 034338 (2012).

[40] D. E. Ward, B. G. Carlsson, and S. Åberg, Phys. Rev. C **92**, 014314 (2015).
[41] G. Audi, F. Kondev, M. Wang, B. Pfeiffer, X. Sun, J. Blachot, and M. MacCormick, Chin. Phys. C **36**, 1157 (2012).
[42] B. Buck, A. C. Merchant, and S. M. Perez, Phys. Rev. C **45**, 2247 (1992).
[43] M. Wang, G. Audi, A. Wapstra, F. Kondev, M. MacCormick, X. Xu, and B. Pfeiffer, Chin. Phys. C **36**, 1603 (2012).
[44] G. Audi, M. Wang, A. Wapstra, F. Kondev, M. MacCormick, X. Xu, and B. Pfeiffer, Chin. Phys. C **36**, 1287 (2012).
[45] N. Wang, M. Liu, and X. Wu, Phys. Rev. C **81**, 044322 (2010).
[46] A. Koning and J. Delaroche, Nucl. Phys. A **713**, 231 (2003).
[47] D. Warner, M. Bentley, and P. Van Isacker, Nat. Phys. **2**, 311 (2006).
[48] B.-A. Li, L.-W. Chen, and C. M. Ko, Phys. Rep. **464**, 113 (2008).
[49] A. W. Steiner, M. Prakash, J. M. Lattimer, and P. J. Ellis, Phys. Rep. **411**, 325 (2005).
[50] A. M. Lane, Nucl. Phys. **35**, 676 (1962).
[51] E. Shin, Y. Lim, C. H. Hyun, and Y. Oh, arXiv:1511.02555.
[52] Y. Z. Wang, J. Z. Gu, and Z. Y. Hou, Phys. Rev. C **89**, 047301 (2014).
[53] K. Rutz, M. Bender, T. Bürvenich, T. Schilling, P.-G. Reinhard, J. A. Maruhn, and W. Greiner, Phys. Rev. C **56**, 238 (1997).
[54] J. Dong, W. Zuo, and W. Scheid, Phys. Rev. Lett. **107**, 012501 (2011).
[55] X. Bao, H. Zhang, H. Zhang, G. Royer, and J. Li, Nucl. Phys. A **921**, 85 (2014).
[56] C. Xu, Z. Ren, and Y. Guo, Phys. Rev. C **78**, 044329 (2008).